Characterization of Mode I and II Interlaminar Fracture Toughness in Onyx/Aramid 3D Printed Composites

Benjamín A. Moreno-Núñez [1], Cecilia D. Treviño-Quintanilla[2], Gonzalo Pincheira-Orellana[3], Enrique Martínez-Franco[4]

[1]School of Engineering and Sciences, Tecnológico de Monterrey, Querétaro, México, [2]Institute of Advanced Materials for Sustainable Manufacturing, Tecnológico de Monterrey, Nuevo León, México, [3]Department of Industrial Technologies, Faculty of Engineering, Universidad de Talca, Curicó, Chile, and [4]Centro de Ingeniería y Desarrollo Industrial (CIDESI), Querétaro, México

INTRODUCTION

In recent years, 3D Printed Composite Materials (3DPCM) have increased their appearance and use in different sectors for the fabrication of ready-for-use products. 3DPCM can combine 3D printed geometries with the mechanical and physical properties of composite materials [1].

Due to the nature of the layer-by-layer additive manufacturing process of 3DPCM, the products obtained can exhibit poor interlaminar bonding [2], resulting in low interlaminar fracture toughness [3] and delamination [4]. This is caused by the bad adhesion between matrix, fibers or layers, having a direct and negative effect on mechanical properties [5].

Interlaminar fracture toughness is an important indicator of impact resistance, crack initiation and it is propagation [6]. In fracture scenarios, 3DPCM have shown unstable crack growth [7]. It has been indicated that further analysis is necessary to optimize interface bonding quality of 3DPCM using different configurations and materials as aramid reinforcement [8].

This research is aimed to analyze Mode I and Mode II interlaminar fracture toughness of Onyx-Aramid 3DPCM, also the interlaminar zone of fractured samples. The results from this research can help to improve and enhance the mechanical properties of 3DPCM when compared to traditional composite materials. Understanding fracture toughness can help to improve interlaminar zones to obtain enhanced ready-to-use 3DPCM.

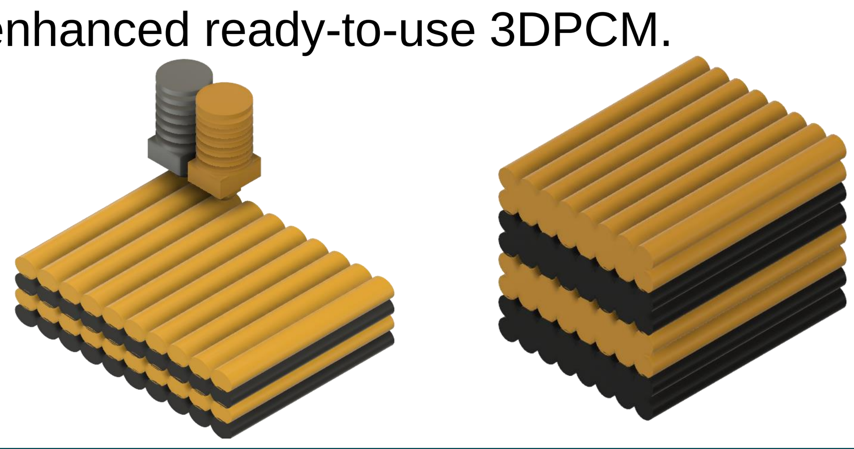

MATERIALS AND METHOD

The samples used in this research were manufactured using Onyx, as matrix, and Aramid fiber, as continuous reinforcement filaments in a MarkTwo™ 3D printer, supplied by Markforged Inc.

Since 3DPCM and additive manufactured composite materials do not have a standard for mechanical behavior evaluation, the standards used were adapted from ASTM standards of reinforced polymers.

The fracture toughness values were obtained using Mode I and Mode II fracture analyses. For Mode I fracture analysis, the standard followed was ASTM D5528, and for Mode II fracture analysis the standard followed was ASTM D7905, as shown in Figure 1.

The reinforcement deposition used in this research for interlaminar fracture toughness analysis were 0° and 90°, as shown in Figure 2, to analyze if this has a direct impact on interlaminar fracture toughness G_I and G_{II} of 3DPCM.

After fracture tests, the samples were optically analyzed using an optical microscope and SEM to analyze the fracture zones and detect defects that caused variations in G_I and G_{II} measurements.

Figure 1. Fracture Modes I (Up), and II(Down).

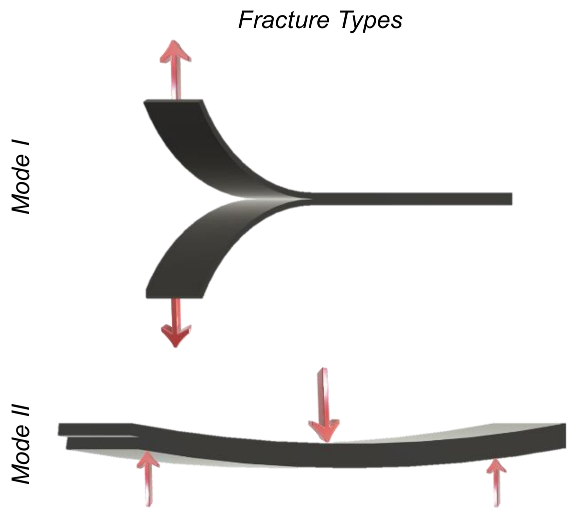

Figure 2. Fiber reinforcement 0°(Up), and 90°(Down).

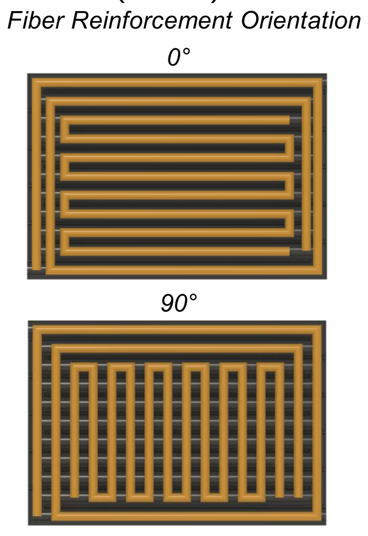

Table 1. 3D printing parameters for fracture samples.

Printing Parameter	Value
Layer Height	0.1 mm
Infill Pattern	Solid
Infill Density	100%
Wall Layers	2
Fiber Angle	0º and 90º
Fiber Volume Fraction	32%
Concentric Fiber Rings	1

ACKNOWLEDGEMENTS

Special acknowledgement to the engineering department of the Universidad de Talca, Campus Curicó for their support in the fracture tests. Also, authors want to acknowledge Centro de Ingeniería y Desarrollo Industrial (CIDESI) for their support in the SEM images acquisitions.

RESULTS AND DISCUSSION

The experimental results revealed low interlaminar toughness, compared to traditional composite materials, in both fracture modes (Figure 4).

For Mode I, the measured critical energy release rates have a mean of $6.15\ kJ/m^2$ and $9.06\ kJ/m^2$ for 0° and 90° orientations, respectively. For Mode II, the measured critical energy release rates have a mean of $0.74\ kJ/m^2$ and $0.53\ kJ/m^2$ for the same orientations.

Figure 3. Mode I (Up) and Mode II (Down) fracture tests.

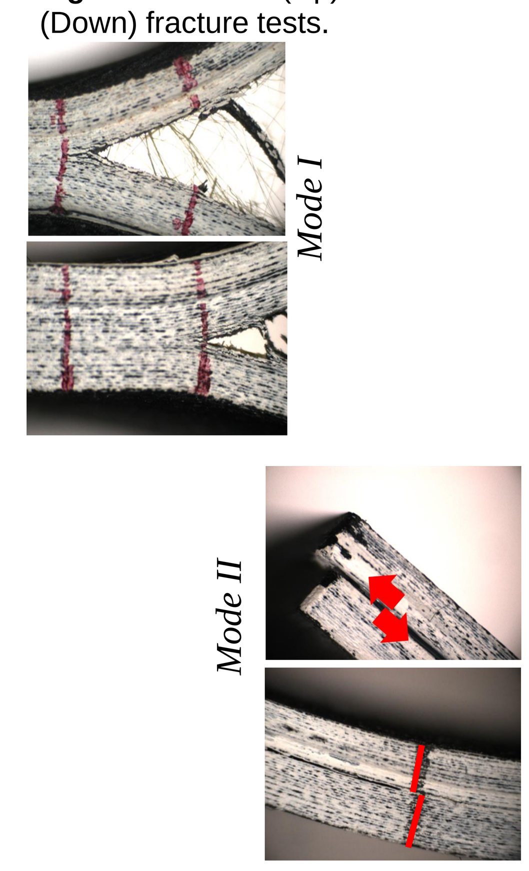

Figure 4. Fracture mode Interlaminar fracture toughness for a) Mode I 0°, b) Mode I 90°, c) Mode II 0°, and d) Mode I 90°

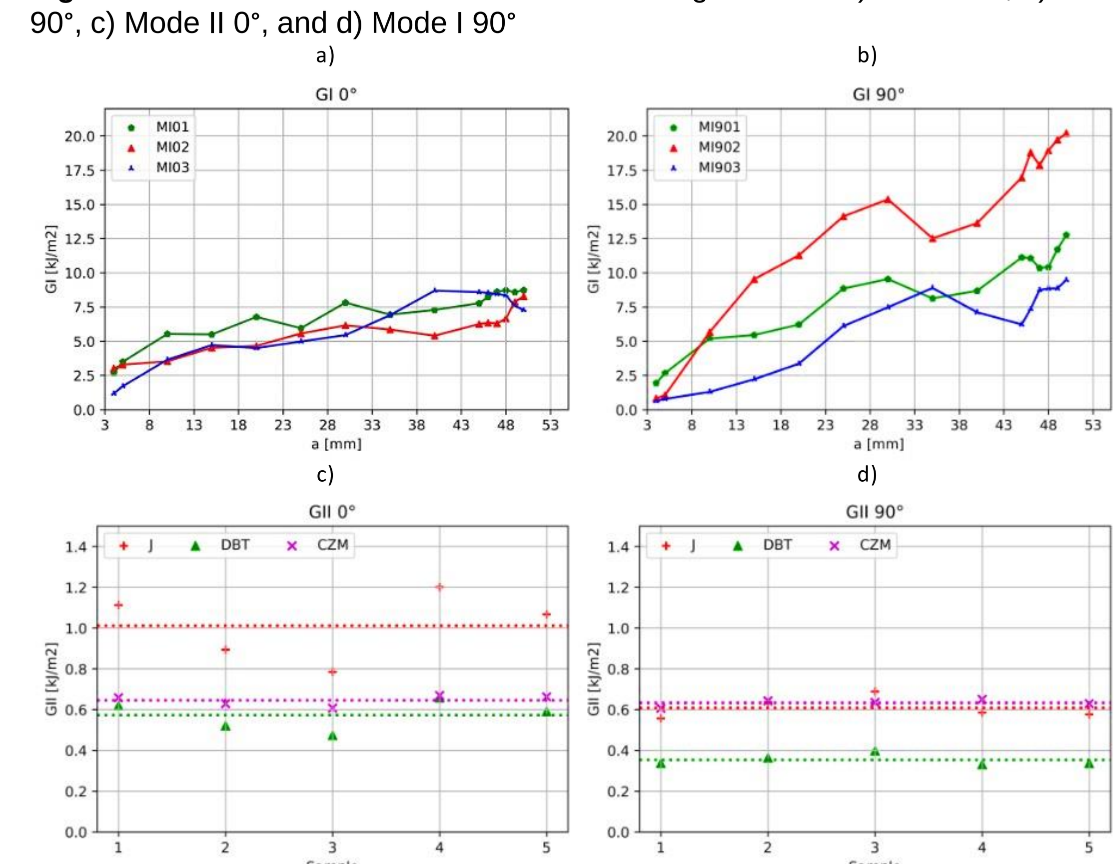

Mode I fracture specimens showed less variation in G_I at 0° compared to G_I at 90°, although G_I at 90° increased notoriously as crack length increased, as seen in Figure 4b. Mode II fracture samples showed similar G_{II} in both reinforcement directions, as seen in Figure 4c (0°) and Figure 4d (90°). The G_{II} in both directions was lower than the G_I in 3DPCMs made with onyx-aramid.

Additionally, specific defects, such as fiber bundle breakage, matrix peeling, unwoven fiber, matrix breakage, matrix gap, fiber exposure, gap between layers, and fiber tearing were identified via SEM (Figure 5), which contribute to the diminished toughness of 3DPCM.

Figure 4. SEM images with defects in post-fractured samples.

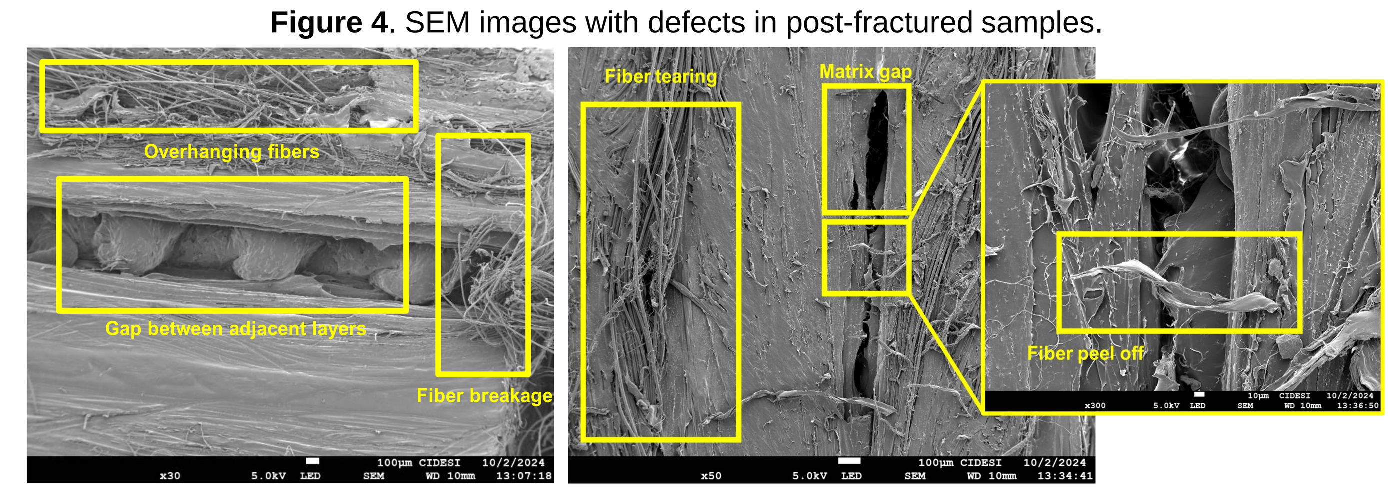

CONCLUSIONS

After the mechanical and optical analyses of the 3DPCMs made with Onyx-Aramid, it was noted that the G_I is higher than the G_{II}, in both, 0° and 90° reinforcement orientations.

Additionally, it was observed that in 0° reinforcement direction, fractures depend on the behavior of the matrix rather than the reinforcement. In 90° samples, the SEM images of the fractured zones showed areas where the matrix was missing, and the reinforcement was unwoven.

Incorporating these observations into 3DPCM analyses could further improve the manufacturing techniques used to manufacture them, leading to improved interlaminar fracture toughness. This could unlock the full potential of 3DPCMs in industries such as aerospace, transportation, and others.

BIBLIOGRAPHY

[1] Tuli NT, Khatun S, Rashid A Bin. Unlocking the future of precision manufacturing: A comprehensive exploration of 3D printing with fiber-reinforced composites in aerospace, automotive, medical, and consumer industries. Heliyon 2024;10:e27328. https://doi.org/10.1016/j.heliyon.2024.e27328.

[3] Pascual-González C, San Martín P, Lizarralde I, Fernández A, León A, Lopes CS, et al. Post-processing effects on microstructure, interlaminar and thermal properties of 3D printed continuous carbon fibre composites. Compos B Eng 2021;210:108652. https://doi.org/10.1016/j.compositesb.2021.108652.

[4] He Q, Wang H, Fu K, Ye L. 3D printed continuous CF/PA6 composites: Effect of microscopic voids on mechanical performance. Compos Sci Technol 2020;191:108077. https://doi.org/10.1016/j.compscitech.2020.108077.

[5] Dang Z, Cao J, Pagani A, Zhang C. Fracture toughness determination and mechanism for mode-I interlaminar failure of 3D-printed carbon-Kevlar composites. Composites Communications 2023;39:101532. https://doi.org/10.1016/j.coco.2023.101532.

[6] Kong X, Luo J, Luo Q, Li Q, Sun G. Experimental study on interface failure behavior of 3D printed continuous fiber reinforced composites. Addit Manuf 2022;59:103077. https://doi.org/10.1016/J.ADDMA.2022.103077.

[8] Saito H, Kikuchi R, Kimpara I. Evaluation of Mode I interlaminar fracture toughness in asymmetric interlayer in CFRP laminates. Advanced Composite Materials 2020;29:163–77. https://doi.org/10.1080/09243046.2019.1669002.

[9] Katalagarianakis A, Polyzos E, Van Hemelrijck D, Pyl L. Mode I, mode II and mixed mode I-II delamination of carbon fibre-reinforced polyamide composites 3D-printed by material extrusion. Compos Part A Appl Sci Manuf 2023;173:107655. https://doi.org/10.1016/j.compositesa.2023.107655.

[10] Swart R, Korkees F, Dorrington P, Thurman J. Evaluation of the impact performance and energy absorption capabilities of 3D printed composites. Rapid Prototyp J 2022;28:1636–54. https://doi.org/10.1108/RPJ-10-2021-0287.

[11] Touchard F, Chocinski-Arnault L, Fournier T, Magro C, Lafitte A, Caradec A. Interfacial adhesion quality in 3D printed continuous CF/PA6 composites at filament/matrix and interlaminar scales. Compos B Eng 2021;218:108891. https://doi.org/10.1016/j.compositesb.2021.108891.